

**Response to Fourth Request for Additional Information – ANP-10285P
“U. S. EPR Fuel Assembly Mechanical Design Topical Report”**

RAI-46. AREVA proposed upper bound growth curve for the EPR fuel assembly (based on the Mark B-HTP data) appears to be based on the following four assumptions: (1) the Mark B-HTP growth data is applicable to the EPR fuel design, (2) the four data points at 50 GWd/MTU is the mean of the EPR growth, (3) there is a linear dependence (or a lesser dependence) of growth with fluence at high burnup, and (4) the variability of the growth data for the Mark B12 and B11 designs represents the upper tolerance bounds of growth for the EPR fuel design. Provide the Mark B12 and B11A data above an assembly burnup of 47 GWd/MTU used to determine the upper tolerance for the EPR fuel design. Provide justification for each of these four assumptions and identify the uncertainty band of the calculated stress history versus exposure presented in Figure 38-5 for each fuel design in this figure.

Response to RAI-46:

The bases for assumption (1) and the uncertainty bands of the calculated stress history for the Mark-B12, Mark-B HTP, and U.S. EPR high thermal performance (HTP) designs are provided in the Response to RAI-47. The Response to RAI-48 addresses the bases for assumptions (2) and (3). The bases for assumption (4) and the requested Mark-B12 and Mark-B11A data are provided in the Response to RAI-49. This response summarizes the information that is detailed in the other responses.

Regarding assumption (1), the Mark-B HTP design is representative of the U.S. EPR HTP design in guide tube stress history. The Response to RAI-38 showed that the Mark-B HTP and U.S. EPR HTP fuel assembly designs are similar in design features. Because Zirconium alloy growth is largely an axial creep-induced response dependent upon the design features and stress state of the guide tubes, the empirically-based Mark-B HTP fuel assembly growth design limits are conservatively applicable to the U.S. EPR fuel assembly design.

Regarding assumption (2), a sufficient amount of empirical growth data ([] measurements) of the Mark-B HTP design, including [] GWd/mtU, exist to provide a conservative estimate of the nominal assembly growth behavior. This estimate of the nominal fuel assembly growth is conservative because it is based on the highest fuel assembly growth rate data observed with the lower growth rate data not included.

Regarding assumption (3), the linear growth rate trend applied to the Mark-B HTP design is consistent with the growth data for all design families after the transition to increased growth occurs. Fuel assembly growth data up to [] GWd/mtU for design families in addition to the Mark-B11A/12, Mark-BW, and Mark-B HTP were examined and also show a linear behavior at higher burnups. The empirically-based Mark-B HTP fuel assembly growth rate trend is also consistent with the linear trend established for M5[®] irradiation free growth data after the transition to increased growth.

Regarding assumption (4), a sufficient amount of data ([] measurements) of the Mark-B fuel design at burnups up to [] GWd/mtU exist to provide an applicable variance estimate for the Mark-B HTP correlation based on 95/95 percent confidence limits. The data used to establish the statistical variance include [] fuel assemblies above a burnup of [] GWd/mtU, in addition to fuel assemblies with growth rates considered to be both nominal and high (such as the TMI-1 batch 16 data). The variance established by the large quantity of

empirical Mark-B fuel assembly growth data represents the inherent variation of all the parameters influencing growth, including guide tube loading/stress state and corresponding axial creep, in addition to material irradiation free growth variation. The variance, which is also shown to be consistent with that of the Mark-BW fuel assembly growth data, is considered to be representative of the Mark-B HTP and the U.S. EPR design.

The information presented in the Response to RAI-47, RAI-48, and RAI-49 further substantiate the four assumptions specified in the Response to RAI-46.

The conclusions defined in the Response to RAI-38 regarding fuel assembly growth remain applicable:

1. The Mark-B HTP fuel assembly design is similar to the U.S. EPR design in guide tube stress history, and the empirically-based Mark-B HTP fuel assembly growth design limits are conservatively applicable to the U.S. EPR fuel assembly design.
2. The use of the Mark-B HTP fuel assembly growth design limits results in a maximum U.S. EPR fuel assembly burnup of 55.7 GWd/mtU, at which the maximum allowable growth of 0.389 percent at cold conditions is obtained.

RAI-47. *The following questions are intended to provide a better understanding of the different stress histories for the different fuel designs that are used to justify the use of the Mark B-HTP design for application to the EPR fuel design.*

- a) *Provide the guide tube stresses induced by each of the following components as a function of fluence/burnup; stresses induced by assembly holddown springs, flow induced stresses, and stresses induced by fuel rod growth that produced the stress versus fluence curve in shown in Figure 38-5 for Mark B12, Mark B-HTP and EPR designs. Separate out the different stress components for each of these design differences. Are there any other stresses considered in this calculation? If so, define these stresses and their differences between the different designs.*
- b) *Provide the uncertainty for each of the stress components in part (a) above for each fuel design.*
- c) *Define the space grid spring relaxation history along with the spring friction coefficients, how they were determined, and uncertainties in both of these parameters for each fuel design.*
- d) *What other design features related to fuel pin design, grid spacer design, top and bottom nozzle design, hold-down leaf-spring design, and guide tube design that impact assembly growth and their relative impact on guide tube stresses (if related to stress). If not related to guide tube stress but are assumed to impact assembly growth, please provide details of how the design feature impacts assembly growth.*
- e) *Based on the above comparisons discuss and demonstrate why only Mark B-HTP design is relevant to EPR.*

Response to RAI-47:

Response to RAI-47(a):

Figure 47-1 provides the nominal average guide tube stress history for the U.S. EPR high thermal performance (HTP), Mark-B HTP, and Mark-B12 fuel designs. The guide tube stress history shown includes the loads due to holddown, hydraulic flow (buoyant component weight), and fuel rod growth (slippage). Other effects included in the stresses are spacer grid irradiation relaxation, guide tube irradiation creep, and guide tube irradiation free growth. Figure 47-2, Figure 47-3, and Figure 47-4 provide the average guide tube stress history for the loads specific to holddown, hydraulic flow, and fuel rod growth (slippage), respectively, for each of the three designs.

Figure 47-2 shows that the guide tube stresses due to the holddown loads are compressive. The compressive loads tend to reduce the growth of the fuel assemblies. The U.S. EPR design has the most compressive stress due to the design's higher net holddown ([]). The Mark-B12 and Mark-B HTP guide tube stresses due to holddown are approximately equal.

The guide tube stresses due to the hydraulic flow loads are tensile as shown in Figure 47-3. The U.S. EPR design has slightly lower guide tube stresses because of the hydraulic loads compared to the Mark-B HTP ([]). This is primarily attributed to the larger (69 percent) guide tube cross section of the U.S EPR design that offsets the higher hydraulic loads. The tensile loads tend to increase the growth of the fuel assemblies.

Of the three parameters, fuel rod slippage, which results from differential fuel rod and guide tube growth, has the largest tensile effect on guide tube stress as shown in Figure 47-4. The tensile loads tend to increase the growth of the fuel assemblies. For fuel rod slippage, the Mark-B12 design has the highest overall tensile stresses over the life of the fuel due to the higher as-designed slip load and lower relaxation of the Inconel 718 end grid spacer springs in conjunction with the fuel rods seated on the bottom nozzle. The corresponding guide tube stresses for the U.S. EPR and Mark-B HTP designs are considerably lower ([] lower for the U.S EPR and [] lower for the Mark-B HTP for fluences from []).

The change in stress state for the U.S. EPR and Mark-B HTP designs at [] is attributed to fuel rods contacting the bottom nozzle. The Mark-B HTP design has lower relative guide tube stress due to fuel rod slippage. In comparing the U.S. EPR and Mark-B HTP designs to the Mark-B12 guide tube stress, the minimum difference exists for a short time at beginning of life. Over the remainder of the operating lifetime, the Mark-B12 guide tube stress is at least [] higher than that of the U.S. EPR and Mark-B HTP designs for the nominal condition.

The net effect of the holddown, hydraulic, and fuel rod slip loads is such that the average guide tube stresses for the Mark-B HTP and U.S. EPR are similar as shown in Figure 47-1 and are well below those of the Mark-B12 design. The differences in guide tube stress state between the Mark-B12 and Mark-B HTP fuel designs are reflected in the higher observed Mark-B12 fuel assembly growth as shown in Figure 48-14.

The lower (more compressive) stress in the Mark-B HTP and U.S. HTP fuel assembly designs supports the conclusion (which is further substantiated by the available data for the Mark-B HTP fuel assembly design) that the fuel assembly growth of these two designs will be lower than the fuel assembly growth of the Mark-B11 and Mark-B12 fuel assembly designs.

Figure 47-1—Comparison of Nominal Guide Tube Stresses



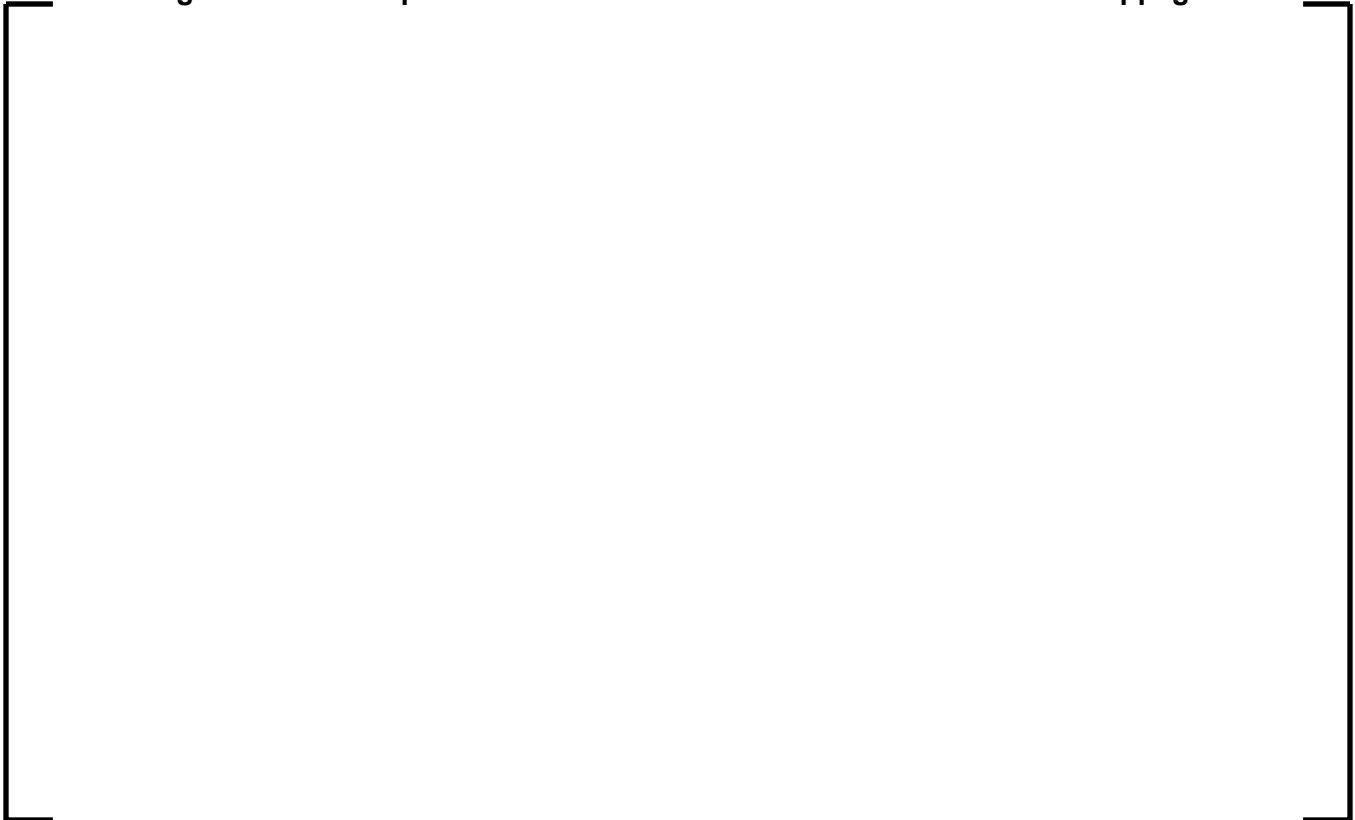
Figure 47-2—Comparison of Guide Tube Stresses Due to Holddown



Figure 47-3—Comparison of Guide Tube Stresses Due to Hydraulic Flow Loads



Figure 47-4—Comparison of Guide Tube Stresses Due to Fuel Rod Slippage



Response to RAI-47(b):

Figure 47-5, Figure 47-6, and Figure 47-7 provide the U.S. EPR average guide tube stress results specific to the holddown, hydraulic, and fuel rod slip loads and corresponding variations, respectively.

The variation for each of the stress components is:

Holddown load	[]
Hydraulic load	[]
Fuel rod slippage load (spacer grid spring friction force)	[]

The variation ranges for the holddown and hydraulic loads are based on the calculated maximum and minimum values when considering input parameter tolerances. The variation range for the fuel rod slip load is described in the Response to RAI-47(c).

Figure 47-5—U.S. EPR Guide Tube Stress Sensitivity to Holddown Variation



Figure 47-6—U.S. EPR Guide Tube Stress Sensitivity to Hydraulic Load Variation



Figure 47-7—U.S. EPR Guide Tube Stress Sensitivity to Fuel Rod Slip Load Variation



Figure 47-8, Figure 47-9, and Figure 47-10 provide comparisons of guide tube stress sensitivity to variations in guide tube free growth, end grid fluence, and fuel rod slip (grid spring friction) load for the Mark-B12, Mark-B HTP, and U.S. EPR designs, respectively. The range of variation is:

Spacer grid fluence and irradiation relaxation	[]
Guide tube irradiation free growth	[]
Fuel rod slippage load (spacer grid spring friction force)	[]

The variation is applied while maintaining all other parameters nominal. The resulting range of guide tube stress variation is comparable for the Mark-B HTP and U.S. EPR designs and is less than that for the higher growth Mark-B12 design.

Figure 47-8—Mark-B12 Guide Tube Stress Sensitivity



Figure 47-9—Mark-B HTP Guide Tube Stress Sensitivity



Figure 47-10—U.S. EPR Guide Tube Stress Sensitivity



Figure 47-11, Figure 47-12, and Figure 47-13 provide comparisons of guide tube stress sensitivity to a variation of [] in guide tube creep while maintaining all other parameters nominal for the Mark-B12, Mark-B HTP, and U.S. EPR designs, respectively. Results show that the variation in average guide tube stress is small.

Figure 47-11—Mark-B12 Guide Tube Stress Sensitivity to GT Creep Variation



Figure 47-12—Mark-B HTP Guide Tube Stress Sensitivity to Guide Tube Creep Variation



Figure 47-13—U.S. EPR Guide Tube Stress Sensitivity to Guide Tube Creep Variation



These evaluations demonstrate that the average guide tube stress is most affected by the variation in fuel rod slip load. Figure 47-14 compares the guide tube stress for the Mark-B12 design with the minimum ([]) fuel rod slip load variation and the Mark-B HTP and U.S. EPR designs with the maximum ([]) fuel rod slip load variation and with all

other parameters defined as nominal. Results show that even for the bounding slip load variation, the U.S. EPR and Mark-B HTP guide tube stresses remain below those of the Mark-B12 for fast fluence greater than [] ([] of the fuel design life). This supports the conclusion that the maximum growth of the Mark-B HTP and U.S. EPR HTP fuel assembly designs are less than that of the Mark-B12 fuel assembly design.

Figure 47-15 compares the guide tube stress for the Mark-B HTP and U.S. EPR designs for maximum ([]) and minimum ([]) fuel rod slip load variation and with all other parameters defined as nominal. Results show that the range of guide tube stress is comparable for the two designs. Thus, the empirically-based Mark-B HTP fuel assembly growth design limits adequately represent the U.S. EPR fuel assembly design and the corresponding variations in stress state.

Figure 47-14—Average Guide Tube Stress Comparison for Bounding Fuel Rod Slip Load Variation



Figure 47-15—Average Guide Tube Stress Comparison for Bounding Fuel Rod Slip Load Variation



Response to RAI-47(c):

Spacer Grid Spring Friction Coefficients

The spacer grid spring preload is the force exerted by one grid spring within a given grid cell on the fuel rod in the beginning of life condition. The preload can be determined by direct measurement, by calculating the interference of the fuel rod and the grid spring and multiplying by the spring stiffness, or by direct measurement of the friction slip load and divide by an appropriate friction coefficient.

The spacer grid slip loads are defined using the following four parameters:

1. The beginning of life (BOL) grid spring preload force, F
2. Coefficient of friction, μ , where Fuel rod slip load = μF
3. Corrective Coefficient for in reactor effects, C
4. Spacer grid spring material relaxation, $R(\Phi t)$

The sliding force as a function of fast fluence (Φt) is then:

[]

C is established at [] for Inconel 718 end grids and [] for zircaloy 4/M5[®] end grids based on correlations with the measured fuel assembly growth data.

For the U.S. EPR, the spacer grid spring forces and slip loads were measured for the 17x17 HTP and 17x17 HMP grids. The empirical range of spring force values was small, i.e., [] percent for the HTP and approximately [] percent for the HMP. []

For the Mark-B HTP, the grid spring force was not directly measured, but was deduced from the spacer grid slip load tests, where the fuel rods are pushed through the spacer grid simultaneously. The maximum variation for the M5[®] HTP grids and Inconel 718 HMP grids is approximately [] percent.

For the Mark-B12 grids, the grid spring force was not directly measured but was also deduced from spacer grid slip load tests. A maximum variation of approximately [] percent was determined from the tests.

In order to conservatively bound these datasets, an uncertainty [] percent is assigned for the spacer grid slip load (spring friction force) variation in the guide tube stress evaluation.

Spacer Grid Spring Irradiation Relaxation History

The spacer grid spring irradiation relaxation history is dependent upon the grid material and fast fluence exposure of the spacer grid. The Mark-B12 and U.S. EPR designs use Inconel 718 for the end grid material with the intermediate grids constructed of Zircaloy-4 and M5[®] respectively. The Mark-B HTP design uses Inconel 718 for the bottom end grid material with the intermediate and top end grid constructed of either Zircaloy-4 or M5[®].

A [] percent uncertainty on the fluence ratios is determined based on MCNP calculations of ratios of neutron fluxes for various elevations of interest, including those corresponding to the end grids outside the active fuel region. The grid spring irradiation relaxation is based on the applicable material and corresponding fluence using the fast fluence ratio.

The sensitivity study is performed varying the end grid fluence [] percent for conservatism. The resulting stress variation is enveloped by that produced with the [] percent uncertainty applied to the spacer grid slip load (see Figure 47-8 to Figure 47-10).

The Inconel 718 grid spring relaxation is based on []
[]. The Inconel 718 grid spring relaxation is defined as follows and is shown graphically in Figure 47-16:

[]; where Φ is the fast fluence E+21 n/cm² and F_o is the initial fuel rod slip load force.

No uncertainty of the Inconel 718 grid spring relaxation law is assigned because the uncertainty assigned to the fluence and grid slip loads provide a conservative assessment of the variance.

Figure 47-16—Inconel 718 Grid Spring Irradiation Relaxation



The grid spring relaxation model for M5[®] and Zircaloy-4 is derived from [], and is defined as follows and shown graphically in Figure 47-17:

[]; where Φ is the fast fluence E+21 n/cm² and F_0 is the initial fuel rod slip load force.

No uncertainty of the M5[®]/Zircaloy-4 grid spring relaxation law is assigned, since the uncertainty assigned to the fluence and spacer grid slip loads provide a conservative assessment of the variance.

Figure 47-17—Zircaloy4/M5[®] Grid Spring Irradiation Relaxation



Response to RAI-47(d):

Design parameters that influence the guide tube stress state include total guide tube cross section area, holddown spring preload and spring rate and corresponding holddown spring irradiation relaxation, hydraulic loads as affected by component pressure drop and bundle flowrate, component buoyant weight, grid slip loads and corresponding spacer grid irradiation relaxation, and lower fuel rod lower shoulder gap closure. These parameters are taken into account in the guide tube stress calculation. Sensitivity evaluations are provided for the predominant parameters in the preceding sections. The variation of these parameters as affected by manufacturing tolerances and processes is exhibited in the scatter of the empirical fuel assembly growth rates observed.

While fuel assembly growth is strongly dependent upon axial creep and guide tube stress, the dimensional stability of all zirconium alloy components is also affected by free growth. The irradiation free growth of a group of Zr1Nb alloy samples representing a wide composition range of the influencing elements was investigated and is shown in Figure 47-18. Table 47-1 gives the chemical composition range of Zr1Nb (including M5[®]) alloys that were specifically investigated for irradiation free growth (under irradiation, free of applied stress). The M5[®] specification controls these elements to an even tighter composition range than that represented by the samples.

Table 47-1—Chemical Composition Range of Free Growth Investigated Samples



Figure 47-18 shows that in the flat growth regime and up to a fluence of [], no significant impact of the chemical composition ranges listed in the table is observed. This fluence range is greater than the highest expected burnup in pressurized water reactors (PWRs).

Response to RAI-47(e):

Results show that the Mark-B HTP and U.S. EPR average guide tube stress histories are comparable both nominally and when considering design variations in holddown load, hydraulic load, grid slip load, end grid fluence/relaxation, guide tube free growth, and guide tube creep. The difference in stress is less than [], with the Mark-B HTP design conservatively more tensile in stress state. There is no overlap of the stress for most of the fuel assembly life even when accounting for the uncertainty in the stress calculation between the Mark-B12 and the Mark-B HTP or U.S. EPR HTP fuel assembly designs. This supports the conclusion that the growth of the U.S. EPR HTP fuel assembly design is bounded by that of the Mark-B HTP fuel design, and both are less than that of the Mark-B12 fuel assembly design.

Based on these stress comparisons, the U.S. EPR fuel design should have growth response within the bounding limits established for the Mark-B HTP design. The variance established by the large quantity of empirical Mark-B fuel assembly growth data represents the inherent variation of all the parameters influencing growth, including guide tube loading/stress state and corresponding axial creep, in addition to material irradiation free growth variation. The variance, which is shown to be consistent with that of the Mark-BW fuel assembly growth data, is considered to be representative of the Mark-B HTP and the U.S. EPR designs.

Figure 47-18—Irradiation Free Growth Data



:

RAI-48. Explain why only four data points at 50 GWd/MTU from Mark B-HTP represents the mean and provide 95/95 confidence to bound the EPR fuel assembly growth at that exposure level or above. Please justify why there is sufficient growth data from Mark B-HTP fuel family to justify the linear dependence of growth above 30 GWd/MTU with 95/95 confidence. Provide details on each of the Mark B-HTP data points including reactor, cycle number and whether the fabrication lot is similar between data points. Fabrication lot can vary depending on the material, or composition ingot from which the guide tube and grid spacer are fabricated, as well as the tooling setup used to make the guide tubes and grid spacers. Define fabrication lots in these terms.

Response to RAI-48:

A total of [] data points exists for the Mark-B high thermal performance (HTP) assembly growth, including [], as shown in Figure 48-1. [] Mark-B HTP data points exist at [] GWd/mtU burnup. The range of assembly growth for the Mark-B HTP design is expected to be lower than that of the Mark-B12 design based on the lower guide tube stress state, which the growth data shown in Figure 48-1 demonstrates. The Mark-B HTP fuel assembly growth is low as defined by the [] measurements. However, the [] measurements indicate a higher growth rate, initiating at burnups above [] GWd/mtU. This type of higher growth rate trend has been [], as illustrated by Figure 48-2. In these cases, the higher growth rate trend appears linear, and has approximately the same slope in the higher burnup range. The empirical data from these high growth rate regimes includes burnups up to [] GWd/mtU. The empirical data from the low growth rate regimes includes burnups up to [] GWd/mtU). There is no assembly growth rate data that suggests a non-linear growth rate within the burnups measured.

Based on this operating experience, there is a condition that can initiate a higher growth rate response of the guide tubes at a burnup of [] GWd/mtU. Thus, the Mark-B HTP best estimate growth model is established conservatively using the higher growth rate [] data (and conservatively not considering the lower growth rate data from []). Given the limited sample size of the high burnup Mark-B HTP data, the upper limit is based on an uncertainty of [] percent $\Delta L/L$, which is calculated using a 95/95 percent confidence limit on the Mark-B (non-HTP) data, that total [] fuel assembly length measurements. The Mark-B data includes the high growth [] shown in Figure 48-1. []

In addition to the empirical fuel assembly growth data, irradiation free growth data on M5[®] and Zr1Nb cladding from [] different reactor experiments are provided in Figure 47-18. The free growth behavior is shown to be basically bi-linear, beginning at a transition fluence range of []. This fluence corresponds to a burnup range of [] GWd/mtU. The linear free growth trend continues beyond the transition fluence up to fluence levels approximately twice those for pressurized water reactor (PWR) fuel and is also consistent with that observed in the fuel assembly growth data even for the higher growth rate data.

Figure 48-1— US Mark-B and Mark-B HTP Assembly Growth Data



Figure 48-2—Global Welded Cage Design Data (AFA-type) Assembly Growth Data



RAI-49. *It appears that the scatter in the Mark B12 and B11 data is used to define the 95/95 tolerance of the Mark B-HTP fuel and EPR fuel. Provide the Mark B12 and B11A data above an assembly burnup of 47 GWd/MTU used to determine the upper tolerance for the EPR fuel design. Provide details on each of the Mark B12 and Mark B11A data points including reactor, cycle number, and whether the fabrication lot is similar between data points.*

Response to RAI-49:

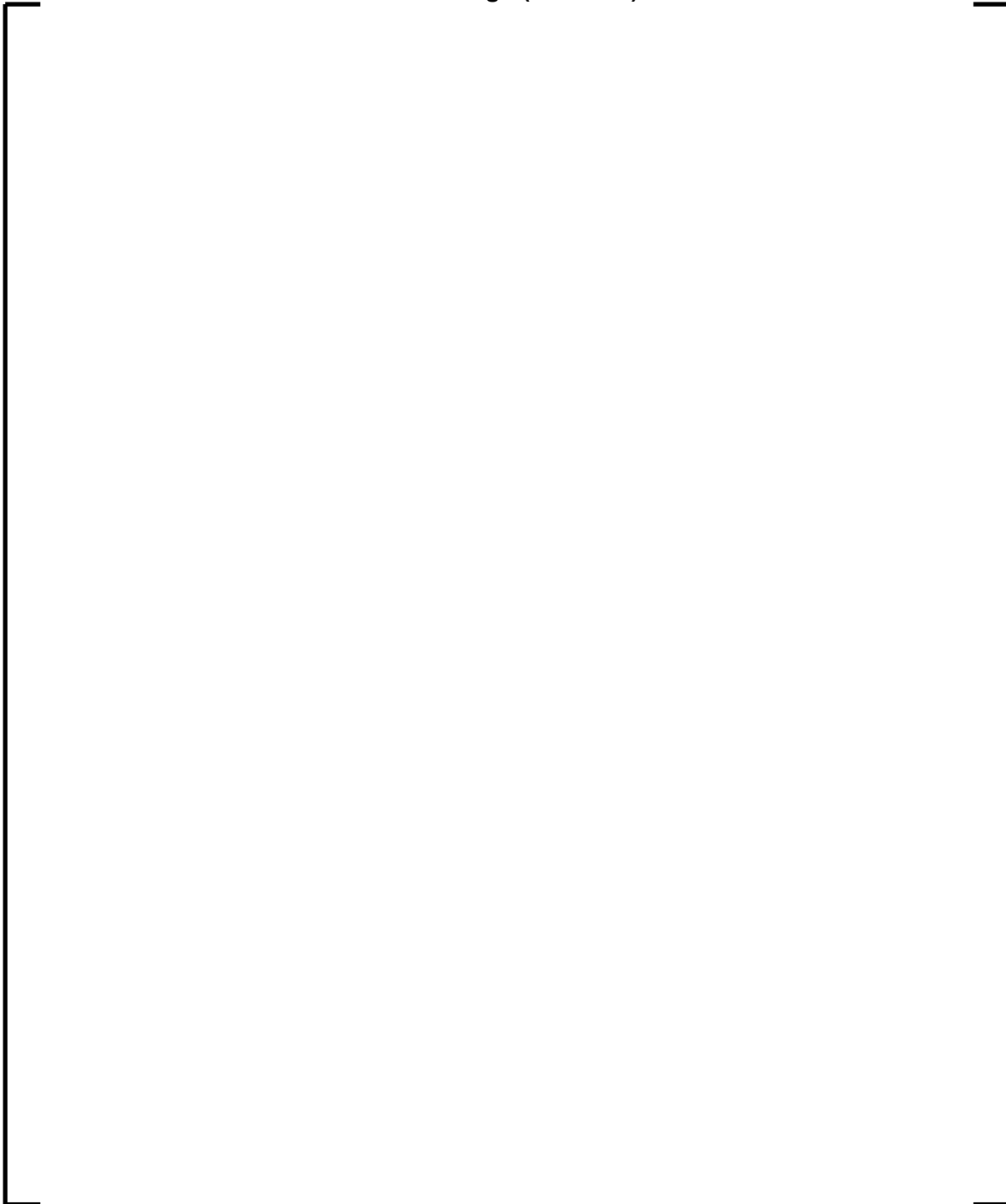
The data used to substantiate a conservative variance for the Mark-B high thermal performance (HTP) assembly growth correlation are shown in Figure 48-1 and provided in Table 49-1. Presently, a total of [] fuel assembly length measurements, including the Mark-B11A, Mark-B10K, and Mark-B12 designs, have been made. These assemblies have M5[®] guide tubes with M5[®] fuel rods. The data encompasses [] . Of these, [] measurements existing at the time of the evaluation ([] of which are equal to or greater than [] GWd/mtU) were used for the statistical evaluation of the variance and also including the high growth TMI-1 Mark-B12 batch 16 fuel.

An uncertainty of [] percent $\Delta L/L$ based on a 95/95 percent confidence limit is calculated from the Mark-B (non-HTP) data, which is shown in Figure 48-1 and is used to establish the Mark-B HTP upper limit. Additional Mark-B HTP fuel assembly length measurements will be obtained in planned future post-irradiation examinations (PIEs) as discussed in the Response to RAI-38 to further expand the data base and validate the growth limits.

Table 49-1—Data to Define the Upper Tolerance Growth Rate for Mark-B-HTP Fuel Design (2 Sheets)



**Table 49-1—Data to Define the Upper Tolerance Growth Rate for Mark-B-HTP
Fuel Design (2 Sheets)**

A large, empty rectangular frame with a thin black border, centered on the page. It is intended to contain the data for Table 49-1, but the content is missing from this page.

RAI-50. *The following question is a follow-up of the staff's evaluation of the response to RAI-42: The response describing the FEA analysis of the top nozzle was inadequate. Provide the ANSYS input files for the top nozzle FEA and describe all conservative assumptions inherent in the analysis, such as un-modeled fillets.*

Response to RAI-50:

The top nozzle analysis was performed with an ANSYS FEA model. Several conservatisms were used in the analysis, as follows:

1. The model used a uniform loading, taking the full 4-g shipping load and distributing this load in a uniform pattern at each guide tube location. The load will try to follow the stiffest load path. Because the center of the plate deflects, higher loadings will be experienced at the guide tube locations closer to the edge of the nozzle. This effect, maldistribution, is well established. Therefore, if higher loads are experienced at the edges and lower loads towards the center, the net deflection of the nozzle surface would be less with maldistribution taken into account. The Membrane + Bending Stresses for the nozzle would be lower, and the resulting margins higher.
2. An actual 4-g shipping load is a short duration, dynamic impact loading. The loads applied in the model are static loads. No provision was made to account for any increase of the material strength from dynamic loadings (i.e., an increase in material strength due to strain rate effects).
3. The supports for the grids inside the shipping container would provide some restraint to the axial motion of the fuel assemblies. However, the analysis assumes that the full 4-g load is being applied to the nozzle.
4. The complete fuel assembly weight was taken to bear on the top nozzle. Reducing the total weight by the weight of the nozzle itself, and calculating a slightly lower 4-g loading, produces an increase in the margin of safety (MS) from 1.4 percent to 2.5 percent.
5. The locations of the highest stresses are in the guide tube boss regions, where the finite element model was simplified by not including fillets which exist in the part. Inclusion of these fillets would not only add additional material to the cross section, but would also remove the artificial sharp corners in the model which increase the local stress concentrations.

A stress convergence study was performed to determine sufficient mesh density on the fuel assembly top nozzle adapter plate to support accuracy of finite element solutions.

The stress sensitivity is based on linear static stress analysis and mesh density dependent under the specific load condition. The results indicate that stress convergence is insignificant as vertical mesh density increased. With increased horizontal mesh density $esize = 0.04$ and vertical mesh density $ethck = 4$ and up, which produces at least four elements across the ligament as well as four elements through the thickness, the static stress solution can achieve stress sensitivity within 1 percent. The U.S. EPR top nozzle analysis was performed with four elements across the ligament and seven elements through the thickness and, thus, used a converged mesh.

The ANSYS input files are provided on a CD. There are two files as follows:

- 1) eprtn.cdb
(This is the ANSYS model CDB file.)

- 2) shipping_handle
(This is the batch file which opens the CDB file, applies the loads, and performs the solution.)

RAI-51. *The following question is a follow-up of the staff's evaluation of the response to RAI-40: The hydrogen levels of the M5 mechanical data used to demonstrate adequate ductility are more than a factor of seven less than the hydrogen limit imposed for M5 cladding. Therefore, the proposed hydrogen limit is not justified for M5 cladding. A revised limit on hydrogen needs to be proposed that is consistent with the mechanical data that exist for fully recrystallized and irradiated M5.*

Response to RAI-51:

Background

AREVA NP does not believe a hydrogen limit is necessary for M5[®] cladding, which this response discusses.

ANP-10285P (Reference 1), Section 5.1.5, states that the upper limit for hydrogen pickup is [] ppm, which is incorrect because there is currently no limit placed on hydrogen content and the value of [] ppm is not applicable to M5[®] cladding. This statement will be deleted from the topical report. In BAW-10227PA (Reference 2), where the use of M5[®] cladding was originally approved, there is no limit placed on the hydrogen content. The words "upper limit" were used in ANP-10285P as well as a value for hydrogen content that is not reflective of M5[®] cladding. AREVA NP was not proposing a limit on the M5[®] cladding hydrogen content with the inadvertent choice of words in the topical report.

BAW-10231PA (Reference 3) (the topical report for COPERNIC) states the following regarding hydrogen content: "An upper bound of the hydrogen content is determined by evaluating the hydrogen content with a maximum zirconium thickness from the corrosion model upper bound." This statement does not impose a limit on the maximum hydrogen content; it specifies how an upper bound on the content for an individual plant can be estimated. In ANP-10285P, Section 5.1.1, the maximum expected corrosion is estimated to be [] microns and the associated upper bound on the hydrogen content is estimated to be approximately [] ppm using the NRC-approved hydrogen upper bound equation. In the safety evaluation for BAW-10231PA, no limitation on the hydrogen content was imposed.

The limit on the corrosion level for M5[®] cladding is [] microns. If the NRC-approved upper bound model for hydrogen content is used for this corrosion level, the maximum hydrogen content would be estimated as approximately [] ppm. This value of hydrogen content is not meaningful because the expected corrosion level for the U.S. EPR M5[®] cladding (and other currently operating reactors) is about [] microns. The estimated maximum upper bound on the hydrogen content at [] microns is about [] ppm. This upper bound is much higher than has been measured for M5[®] cladding at exposures greater than the licensed burnup for M5[®] cladding of 62,000 MWd/tU.

This discussion illustrates why the NRC approval of M5[®] cladding did not impose a limit on the hydrogen content because the expected (based on a significant experimental database) hydrogen content is so low that the impact of small variations in the hydrogen content would not significantly affect the performance of the cladding. AREVA NP is not proposing a limit on the

hydrogen content. The NRC-approved upper bound hydrogen content model will continue to be used to estimate the upper bound hydrogen content of M5[®] cladding.

The uniform elongation data as a function of burnup and fast fluence for irradiated M5[®] cladding at 20° C, 25° C, and 350°C was provided to the NRC in the Response to RAI-40 (prior to that, total elongation was provided in the Response to RAI-28). In the Response to RAI-40, a graph (repeated here as Figure 51-1) depicting the measured M5[®] cladding hydrogen content as a function of burnup was also presented. The data presented in the graph demonstrated that the hydrogen content at burnups exceeding current licensed limits does not exceed 100 ppm.

The discussion and data in this response demonstrate that M5[®] cladding retains its ductility at the low hydrogen concentrations that exist in the cladding. Data that demonstrates sufficient ductility is retained at hydrogen concentrations in excess of what can actually be reached under current operating conditions is also presented.

This response is presented in two parts. The first part updates the data table presented in the Response to RAI-40 with additional data: hydrogen content and total elongation. This section demonstrates the consistently low hydrogen content of M5[®] cladding up to burnups beyond current licensed limits.

The second part of this response demonstrates that sufficient ductility is retained at hydrogen concentrations in excess of what can actually be reached under current operating conditions. There are no M5[®] cladding uniform elongation results at hydrogen contents significantly above those shown in Figure 51-1, and this demonstration makes use of M5[®] guide tube data and total elongation data.

M5[®] Hydrogen Pick-Up

M5[®] cladding in the completely recrystallized condition (RXA) is intrinsically limited in the amount of hydrogen it can absorb in pressurized water reactor (PWR) normal operating conditions up to high burnups. This is because of the low amount of hydrogen available due to the oxidation kinetics of the alloy and the low hydrogen pick-up fraction due to the composition and stable microstructure of the alloy itself.

Table 51-1 presents hot cell hydrogen data and its evolution with burnup and fluence. Figure 51-1 and Figure 51-2 are plots of cladding hydrogen content for M5[®] and Zr-4 and cladding oxidation for M5[®] and Zr-4 respectively. Figure 51-1 was also presented in the Response to RAI-40.

The data presented in Table 51-1 and Figure 51-1 demonstrates that the evolution of hydrogen uptake in M5[®] cladding is linear and increases only slightly with increasing burnup and fluence. This is primarily because the oxidation rate of the M5[®] alloy is low and the hydrogen pickup fraction for the alloy is low (between [] percent at low to high burnup). Depending on the reactor operating conditions, the typical end of life oxide thickness on M5[®] cladding is between [] microns.

The source of hydrogen available to diffuse into the cladding is primarily (almost exclusively) the hydrogen generated in the metal/water corrosion reaction. The low oxidation rate of M5[®] results in a low amount of hydrogen available for migration. Combined with the low hydrogen pickup fraction that results in the low hydrogen content observed in Figure 51-1, at PWR operating

temperatures the cladding hydrogen content, even at the highest burnups achieved, is below the solubility limit for hydrogen in M5[®] cladding. This means that there is no hydride in the M5[®] cladding microstructure during operation. The amount of hydride precipitated during reactor cooldown is observed in Figure 51-1 to be low. This hydride is returned to solution upon heating during subsequent reactor startups. It is a property of alloy M5[®] that during reactor operation, it is not possible to embrittle M5[®] with hydrogen because there is no hydride in the lattice.

Table 51-1—Alloy M5[®] ductility data with temperature, burnup and hydrogen content

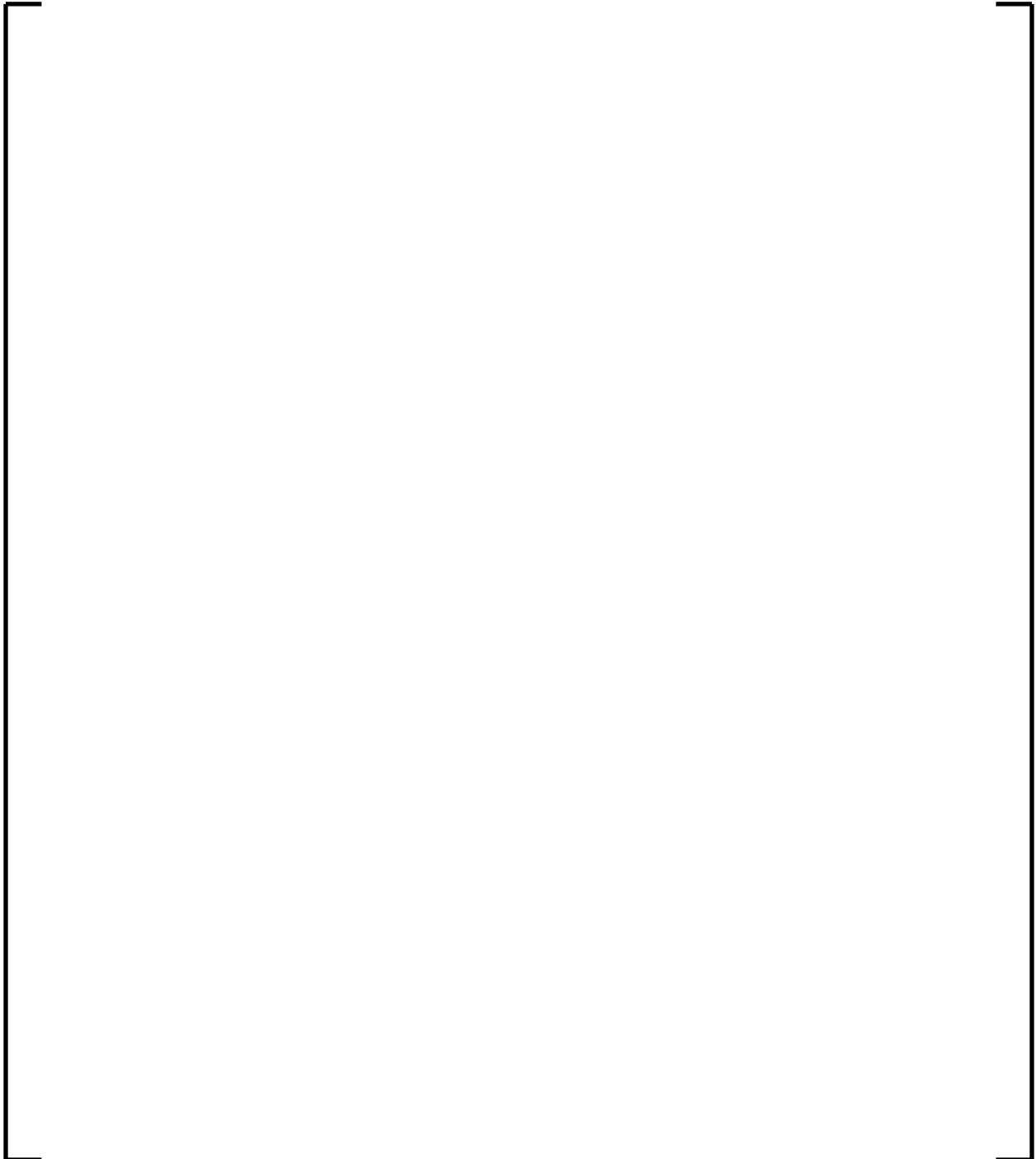
A large, empty rectangular frame with a thin black border, positioned centrally on the page. It is intended to contain the data for Table 51-1, but the content is missing.

Figure 51-1—Hydrogen Evolution in Alloy M5[®] with Increasing Burnup

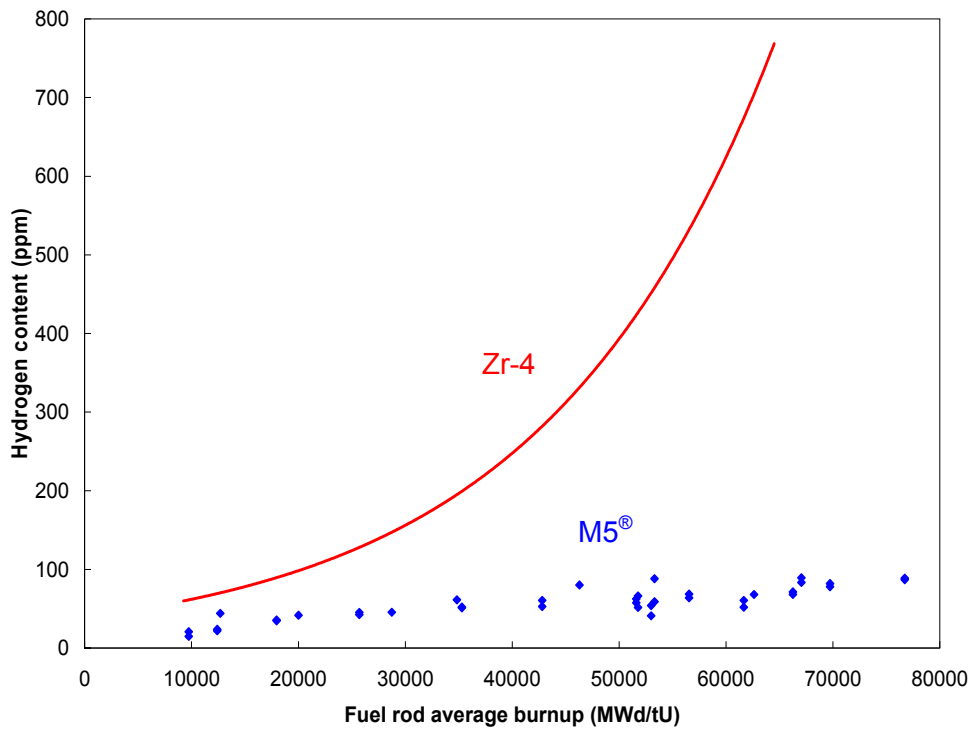
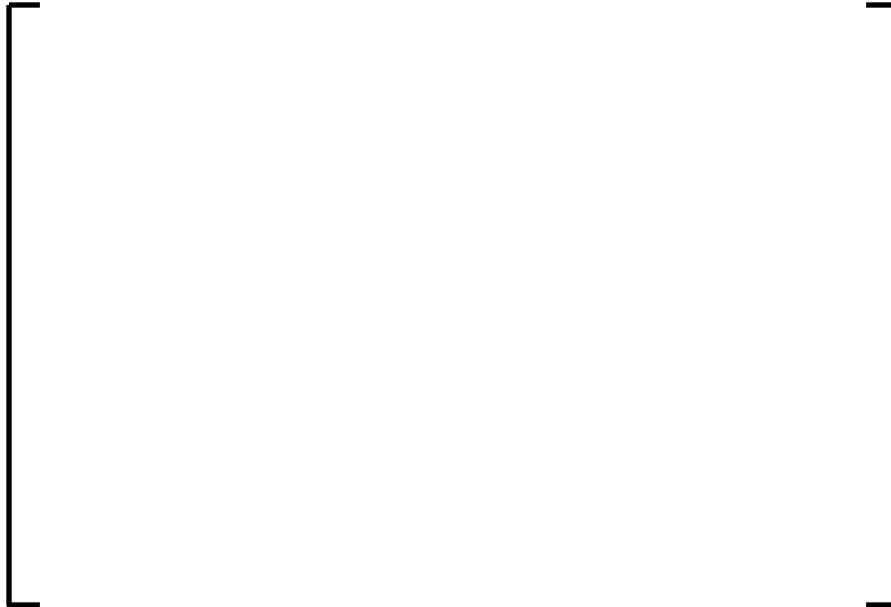


Figure 51-2—Oxidation of Alloy M5[®] with Increasing Burnup



The microstructure of the M5[®] alloy is established by a closely controlled chemical composition and a low temperature manufacturing process. These two factors combine to produce a cladding microstructure with beta niobium second phase particles that remain crystalline during irradiation and retain their size, composition (80 percent Nb), and distribution in the lattice. This means that the alloy's oxidation kinetics do not change significantly with increasing burnup and fluence, which is observed in Figure 51-2.

M5[®] Cladding Behavior with High Hydrogen Content

During reactor operation, the mechanical properties of M5[®] cladding change as a result of the effects of neutron irradiation and hydrogen uptake. Neutron irradiation results in an increase in mechanical strength and a decrease in ductility. The design verification of alloy M5[®] for fuel rod cladding and fuel assembly structural components must take these changes in material properties into account.

Effect of Neutron Irradiation

Under irradiation, M5[®] exhibits the lattice damage deformation that increases its ultimate strength (UTS) and yield strength (YS). At the beginning of life (BOL), the ductility decreases accordingly until reaching a plateau that extends to end of life (EOL). This is exhibited in Figure 51-3 for M5[®] cladding using both uniform elongation and total elongation data.

Figure 51-3—Effect of irradiation on the total and uniform elongation at room and elevated temperature for alloy M5[®]



Effect of Hydrogen Content on Unirradiated M5[®]

As-manufactured M5[®] cladding has an initial hydrogen content of approximately []. As discussed in this response, during reactor operation, a fraction of the hydrogen released as a consequence of alloy corrosion is absorbed by the material. The hydrogen content in M5[®] cladding and its oxide layer thickness increases proportionally to its residence time in the reactor. A detailed investigation was performed on the effects of hydrogen content on the mechanical properties of unirradiated M5[®] alloy. It was found that hydrogen content ranging from [] ppm has no effect on the strength of the alloy at room temperature (20-25°C) or at elevated temperature (350°C).

Ductility is expected to be affected by hydrogen content, which is confirmed. At hydrogen content up to approximately [] ppm, the total elongation at failure of room temperature cladding dropped to approximately [] (tensile test) of their initial values. At elevated temperature, for the same range of hydrogen uptake, the ductility is only slightly affected, which is shown in Figure 51-5 using data on M5[®] guide tubes.

Cumulative Effect of Irradiation and Hydrogen Content

As the investigations on unirradiated M5[®] alloy show, hydrogen content approximately in the range of [] ppm has no effect on material strength at room or elevated temperature

(Figure 51-4). Increases in ultimate strength and yield strength are attributable to irradiation. Likewise, the ductility of M5[®] decreases under the effects of irradiation. At room temperature, irradiation is the dominant factor leading to a significant reduction of ductility at low burn up (< 12000 MWd/tU) that then remains relatively constant regardless of the hydrogen content. This agrees with the general knowledge of the effects of irradiation on the ductility of zirconium alloys exposed to irradiation. When unirradiated and irradiated M5[®] alloy (cladding and guide tube data) at operating temperature are compared (Figure 51-5 and Figure 51-6), it is found that, at hydrogen contents up to approximately [] ppm, irradiation has the dominant effect on ductility loss. Figure 51-5 shows the total elongation at failure of unirradiated M5[®] to range between about [], whereas the values of total elongation at failure (Figure 51-3) for irradiated M5 reach a plateau (compared to the decrease between 0 and 12,000 MWd/tU) beyond approximately 12000 MWd/tU burnup. The inherent scatter of the measured data should be considered. The variability of uniform elongation measurements can be seen in Figure 51-5 by observing the range in as-built M5[®] cladding ductility exhibited in the seven data points at the far left of the plot (no pre-charged hydrogen).

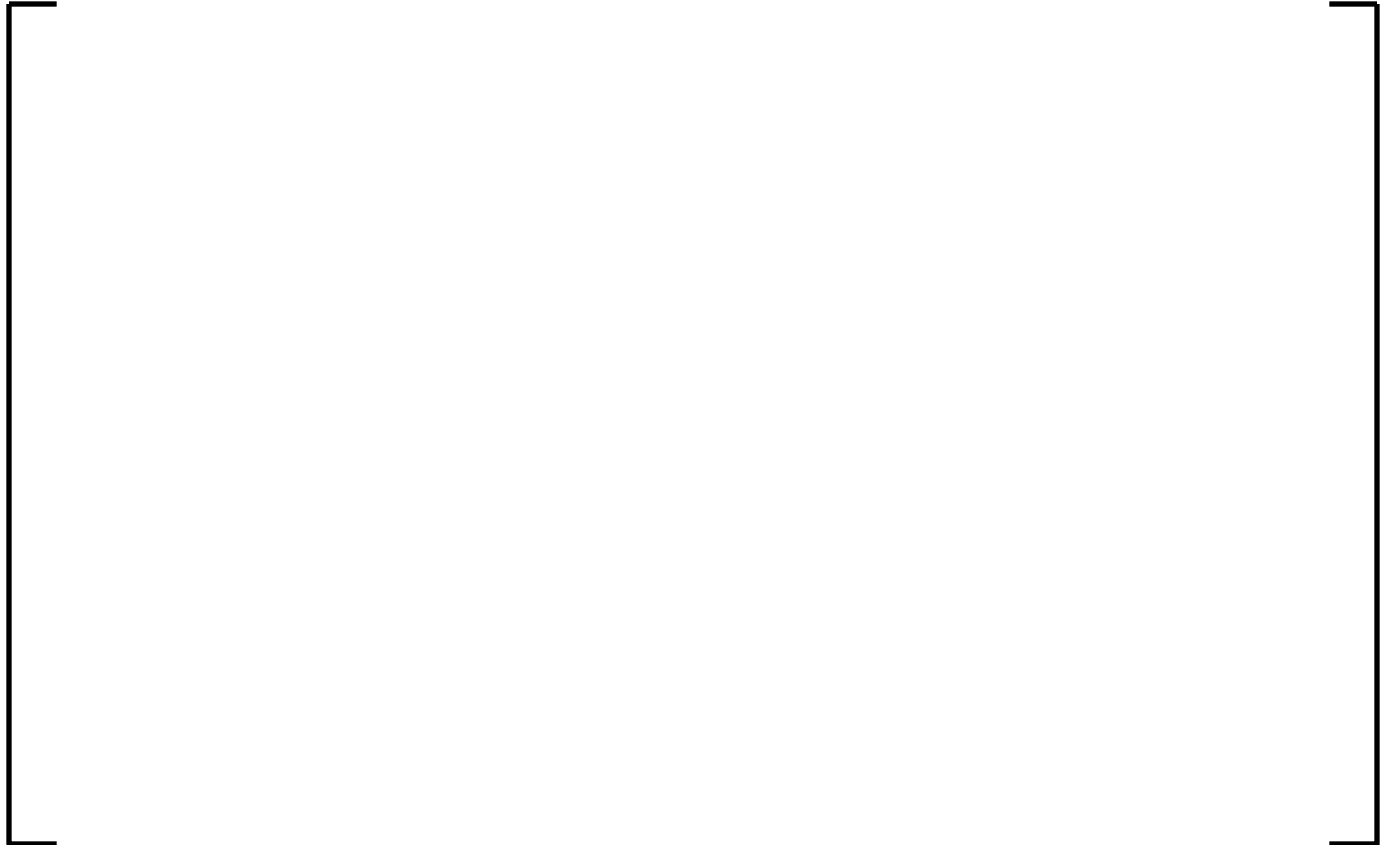
Figure 51-4—Effects of hydrogen content on tensile strength at 350 °C of unirradiated alloy M5[®]



Figure 51-5—Effect of hydrogen content on the ductility of unirradiated alloy M5[®] guide tubes



Figure 51-6—Combined effects of irradiation and hydrogen content on the uniform and total elongation of alloy M5[®] at elevated temperature



Conclusion

The mechanical properties of alloy M5[®] with hydrogen contents achieved under PWR operating conditions and at high levels of hydrogen content (much higher than experienced in alloy M5[®] in a PWR) have been studied. There is no relevant loss of cladding ductility during reactor operation due to hydrogen content. Further, the decrease in ductility from BOL to EOL under the combined effects of hydrogen and irradiation do not violate the minimum ductility requirement of 1 percent uniform elongation. Therefore, the current NRC-approved topical reports which do not impose a limit on the hydrogen content are acceptable. The characteristics of the M5[®] alloy are sufficient to assure that the hydrogen content remains at an acceptable level.

References for RAI 51

1. ANP-10285P Revision 0, "US EPR Fuel Assembly Mechanical Design Topical Report," October 2007.
2. BAW-10227PA Revision 1, "Evaluation of Advanced Cladding and Structural Material (M5) in PWR Reactor Fuel," June, 2003.
3. BAW-10231PA Revision 1, "COPERNIC Fuel Rod Design Computer Code," January 2004.